PCCP

RSC Publishing

PAPER

View Article Online
View Journal | View Issue

Cite this: *Phys. Chem. Chem. Phys.*, 2013, **15**, 12040

New insight into the enhanced visible-light photocatalytic activities of B-, C- and B/C-doped anatase TiO_2 by first-principles

Jiaguo Yu,* Peng Zhou and Qin Li

The geometry structures, formation energies and electronic properties of the B-, C- and B/C-doped anatase TiO_2 were investigated by the density functional theory (DFT) calculations of first-principles. The results indicated that the visible-light absorption and photocatalytic activities of the B-, C- and B/C-doped anatase TiO_2 were not only influenced by the energy gaps (E_g) and the distributions of impurity states, but also affected by the locations of Fermi levels (E_F) and the energies of the edges of band gaps (E_v for the top of valence bands and E_c for the bottom of conduction bands). However, the above four factors changed with the doped models of TiO_2. The impurity states in the band gaps reduced the maximum energy gaps in the band gaps, which is responsible for the absorption of visible light. The Fermi levels at the bottom of conduction bands indicated the existence of Ti^{3+} ions, which enhanced the separation rates of photogenerated electrons and holes. Further, the energies of the edges of band gaps, determining the dominant types of oxidants (O_2^-, hole, $^{\bullet}OH$) in the photocatalytic degradation, were discussed. Moreover, the stability of the doped TiO_2 depended on its growth conditions (O-rich or Ti-rich environment). The O-rich growth condition is beneficial to the substitutional B and C atoms to Ti atoms, while the Ti-rich growth condition is favorable to the other doped TiO_2 including the most stable co-doped TiO_2 with the interstitial B atom and the substitutional C atom to O atom. In addition, our results also showed that the B/C-doped TiO_2 inherited the partial electronic properties of single-doped TiO_2, but also exhibited many new electronic properties, implying that the electronic properties of co-doped systems are not a mechanical mixture of those of both single-doped systems.

Received 22nd December 2012,
Accepted 4th February 2013

DOI: 10.1039/c3cp44651d

www.rsc.org/pccp

1. Introduction

Since Fujishima and Honda reported the photocatalytic hydrogen production by splitting of water on TiO_2 electrodes in 1972,[1] titanium dioxide and other semiconductor photocatalytic materials have been intensively investigated for their wide potential applications in photodecomposition of organic and inorganic contaminants,[2] photosynthesis of organic compounds from carbon dioxide and other inorganic substrates,[3] photodecomposition of water to hydrogen and oxygen,[4] and photoreduction of dinitrogen to ammonia.[5] Among the various oxide and nonoxide semiconductor photocatalysts, titania has proven to be the most suitable for widespread environmental and energy applications due to its biological and chemical inertness, strong oxidizing power, cost-effectiveness, and long-term stability against photocorrosion and chemical corrosion.[6]

However, a large intrinsic band gap of TiO_2 (3.2 eV for anatase and 3.0 eV for rutile) allows only a small portion of the solar spectrum in the ultraviolet (UV) light region to be absorbed.[7] Usually, sunlight contains about 4% ultraviolet light and 43% visible light. Therefore, the effective utilization of visible light has become one of the most important goals in photocatalytic applications. Various methods have been developed to reduce the band gap of TiO_2 *via*, for example, substitutional doping (N, F, P, S, Ni, Sr, Zr *etc.*),[8] and sensitize TiO_2 with organic dyes or narrow-gap semiconductor quantum dots (QDs), such as CdS, CdSe, InP, and PbS QDs.[9]

Recently, many studies indicate that B- and C-doping are promising approaches for inducing visible-light absorption.[10–14] For instance, the visible-light active C-doped TiO_2 was intensively investigated by other groups, also including our group.[15,16] The synthesis and enhanced visible-light photocatalytic activity of the B-doped TiO_2 are also widely reported. This is mainly due

State Key Laboratory of Advanced Technology for Material Synthesis and Processing, Wuhan University of Technology, Wuhan, 430070, P. R. China. E-mail: jiaguoyu@yahoo.com; Fax: 0086-27-87879468; Tel: 0086-27-87871029

to the fact that the B and C atoms with small radii are easily doped into the crystal structure of anatase TiO_2, leading to low formation energies of B- and C-doped anatase TiO_2. Furthermore, Wu *et al.* reported that B/C-doped TiO_2 presented higher visible-light photocatalytic activity than pure, B-doped and C-doped TiO_2 due to the synergistic effect of B and C atoms.[17] Very recently, we also synthesized the B/C-doped TiO_2 and found that the defects induced by the impurity atoms resulted in the higher visible-light photocatalytic activity of the B/C-doped TiO_2 compared to the single-doped TiO_2.[18]

Furthermore, some theoretical studies suggested that the enhanced visible-light photocatalytic activities of the B- and C-doped TiO_2 are ascribed to the narrowing of the band gap.[19] However, Serpone argued that the visible-light photocatalytic activities of doped TiO_2 (including B and C doping) were due to the impurity state in the band gap and not to the decrease of the energy gap.[20] However, there is no related theoretical study performed on the mechanism of visible-light absorption and the photocatalytic activity of the B/C-doped TiO_2.

Herein, for the first time we systematically investigate the geometry structures, formation energies and electronic properties of the B-, C- and B/C-doped anatase TiO_2. The most stable doped model of B/C-doped TiO_2 is determined by the calculations of geometry structures and formation energies. The origin of visible-light absorption and photoactive enhancement for the B-, C- and B/C-doped TiO_2 is investigated and discussed by considering the changes in energy gaps, distributions of the impurity states, locations of Fermi levels and energies of the band edges. This study will provide new insights into understanding the mechanism of visible-light absorption and photoactive enhancement for doped TiO_2 and designing new photocatalytic materials.

2. Computational details

DFT calculations were performed using CASTEP package[21] on the basis of the plane-wave-pseudo-potential approach. The Perdew–Burke–Ernzerhof (PBE) of the generalized gradient approximation (GGA) was used as the exchange–correlation function.[22,23] The interaction between valence electrons and the ionic core was described by the ultrasoft pseudo-potential. To simulate the different doping patterns of B and C elements in anatase TiO_2, we considered B and C atoms substituting lattice atoms (O and Ti atoms) and occupying the interstices in the $2 \times 2 \times 1$ supercells (containing 16 Ti atoms and 32 O atoms, see Fig. 1). In the single-doped TiO_2 models, one impurity atom (B or C) in the forms of a substitutional atom (B_O or C_O) to the O atom, a substitutional atom (B_{Ti} or C_{Ti}) to the Ti atom and an interstitial atom (B_i or C_i) was, respectively, doped into the supercells of TiO_2. But in the B/C-doped TiO_2 models, one B atom (B_O, B_{Ti} or B_i) and one C atom (C_O, C_{Ti} or C_i) are simultaneously doped into the supercell of TiO_2, which resulted in nine different kinds of B/C-doped TiO_2 models. Furthermore, to eliminate the direct bonding interaction between B and C atoms in the co-doped TiO_2 models, we kept the two impurity atoms dispersed as soon as possible.

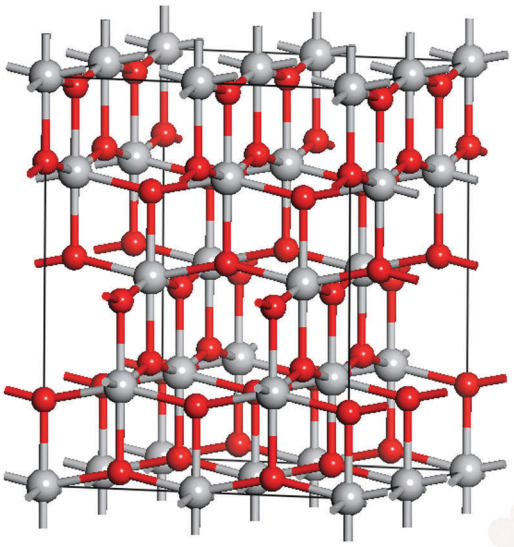

Fig. 1 The geometry structures for the $2 \times 2 \times 1$ supercell. The big gray spheres represent Ti atoms and the small red spheres represent O atoms.

The doping concentration (mole ratio) of the B (C) atom ranges from 2.08% for existing two substitutional atoms to 2.00% for existing two interstitial atoms, comparable to those used in some experiments.[17,18] The geometry optimizations were performed under the cutoff energy for 400 eV, the Monkhorst–Pack *k*-point mesh for $4 \times 4 \times 4$ and the self-consistent field for 5×10^{-5} eV per atom.[24] The convergence tolerance parameters of optimized calculations were an energy of 2.0×10^{-5} eV per atom, a maximum force of 0.05 eV $Å^{-1}$, a maximum stress of 0.1 GPa and a maximum displacement of 0.002 Å. In order to examine the accuracy of the calculations, we adopted higher cutoff energy and more *k* points, the results of which showed almost no change in the energy and geometry structure. After finishing the geometry optimizations, the band structures and the projected density of states (PDOS) of doped anatase TiO_2 were calculated.

3. Results and discussion

3.1 Optimized structures

In this work, the pure, B-doped, C-doped and B/C-doped anatase TiO_2 were studied. The partial geometry structures from the optimized $2 \times 2 \times 1$ supercells of anatase TiO_2 are shown in Fig. 2. For the B-doped TiO_2, the B_O atom (see Fig. 2a) is bonded to two adjacent Ti atoms, the B_{Ti} atom (see Fig. 2b) bonded to four adjacent O atoms forming a body-centered tetrahedron and the B_i atom (see Fig. 2c) also bonded to four adjacent O atoms like a flattened body-centered tetrahedron. For the C-doped TiO_2, the C_O atom (see Fig. 2d) is still bonded to three adjacent Ti atoms, the C_{Ti} atom (see Fig. 2e) bonded to two O atoms forming a linear CO_2 molecule similar to that reported by Dai *et al.*[19b] and the C_i atom (see Fig. 2f) not bonded to any atoms. But in the B/C-doped TiO_2 except the B_OC_O–TiO_2 (see Fig. 2g) and B_iC_O–TiO_2 (see Fig. 2m), the B and C atoms

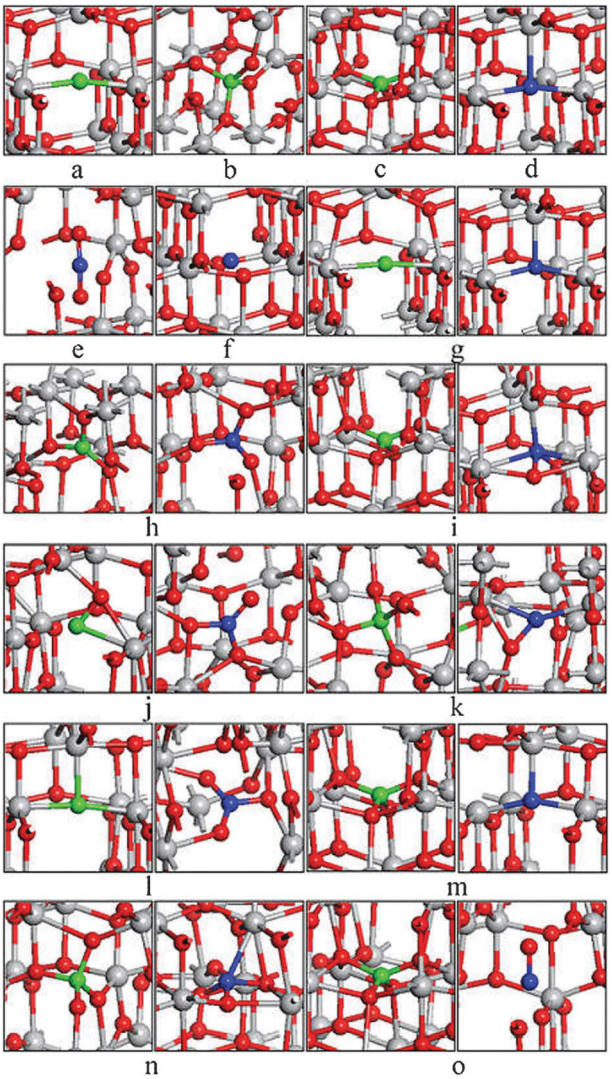

Fig. 2 The partial geometry for optimized structure: (a) B_O–TiO_2, (b) B_{Ti}–TiO_2, (c) B_i–TiO_2, (d) C_O–TiO_2, (e) C_{Ti}–TiO_2, (f) C_i–TiO_2, (g) B_OC_O–TiO_2, (h) $B_{Ti}C_{Ti}$–TiO_2, (i) B_iC_i–TiO_2, (j) B_OC_{Ti}–TiO_2, (k) $B_{Ti}C_O$–TiO_2, (l) B_OC_i–TiO_2, (m) B_iC_O–TiO_2, (n) $B_{Ti}C_i$–TiO_2, (o) B_iC_{Ti}–TiO_2. The order numbers in later tables and figures also follow the same regulation. The gray spheres stand for Ti atoms, the red spheres for O atoms, the green spheres for B atoms, and the blue spheres for C atoms.

Table 1 Optimized cell parameters and bond lengths in B-, C- and B/C-doped anatase TiO_2[a]

No.	Doped TiO_2	Structure parameter (Å)			Bond length (Å)			
		a	*b*	*c*	B–O	B–Ti	C–O	C–Ti
(a)	B_O	3.776	3.776	9.486		$2.075_{eq}(2)$[b]		
(b)	B_{Ti}	3.785	3.838	9.945	1.470			
					1.490			
					1.503			
					1.540			
(c)	B_i	3.776	3.776	9.486	1.501(4)			
(d)	C_O	3.776	3.776	9.486				$1.974_{eq}(2)$
								2.185_{ax}
(e)	C_{Ti}	3.875	3.874	10.035			1.181	
							1.180	
(f)	C_i	3.817	3.817	9.886				
(g)	B_OC_O	3.829	3.833	9.988		$2.146_{eq}(2)$		$1.965_{eq}(2)$
								1.980_{ax}
(h)	$B_{Ti}C_{Ti}$	3.850	3.863	9.954	1.373		1.270	
					1.391		1.312	
					1.411		1.322	
(i)	B_iC_i	3.838	3.833	10.069	1.495			2.075_{eq}
					1.499		1.404	2.116_{ax}
					1.503		1.423	2.308_{eq}
					1.504			
(j)	B_OC_{Ti}	4.006	3.788	10.172	1.362	2.207_{eq}	1.242	
							1.342	
							1.348	
(k)	$B_{Ti}C_O$	3.778	3.822	10.124	1.480			
					1.498		1.311	2.086_{eq}
					1.517			2.088_{eq}
					1.522			
(l)	B_OC_i	3.973	3.808	9.918		2.012_{eq}	1.294	
						2.023_{eq}	1.295	
						2.026_{ax}	1.306	
(m)	B_iC_O	3.843	3.798	10.006	1.488			1.903_{eq}
					1.500			1.917_{ax}
					1.511(2)			1.921_{eq}
(n)	$B_{Ti}C_i$	3.806	3.848	9.957	1.470		1.409	
					1.482		1.428	2.248_{ax}
					1.504		1.451	
					1.573			
(o)	B_iC_{Ti}	3.789	3.883	10.214	1.489(2)		1.191	
					1.515(2)			

[a] In pure anatase TiO_2: $a = b = 3.776$ Å, $c = 9.486$ Å, equatorial Ti–O = 1.959 Å and axial Ti–O = 2.004 Å. [b] The numbers in the parentheses show the quantity of bonds with same length.

do not continue to maintain the initial coordination mode in the single-doped TiO_2, which implies indirect interactions between the B and C atoms. Table 1 summarizes the optimized cell parameters and bond lengths for all doped TiO_2 models. In the pure anatase TiO_2, the cell parameters *a* and *c* are 3.776 and 9.486 Å, respectively. In the single-doped TiO_2, the cell parameters of B_O–TiO_2, B_i–TiO_2 and C_O–TiO_2 are still equal to those of pure TiO_2, but the cell parameters of the B_{Ti}–TiO_2, C_{Ti}–TiO_2 and C_i–TiO_2 expand to different degrees. However, the cell parameters of all B/C-doped TiO_2 become bigger than those of pure TiO_2, which is in agreement with the experimental results reported by Wu *et al.*[17a] The extensions of cell parameters in the doped TiO_2 are considered from the changes in the lengths of bonds. In the pure TiO_2, the lengths of equatorial Ti–O and axial Ti–O are 1.959 and 2.004 Å, respectively. However, the B–Ti and C–Ti bonds in the doped TiO_2 except B_OC_O–TiO_2 and B_iC_O–TiO_2 are longer than corresponding O–Ti bonds in the pure TiO_2, owing to the smaller binding energies of B–Ti and C–Ti bonds. Besides, though the B–O and C–O bonds are shorter than initial O–Ti bonds, the directions of the B–O and C–O bonds changed significantly, thus resulting in obvious lattice distortions. This can also explain the extension of the cell parameters in the B_OC_O–TiO_2 and B_iC_O–TiO_2 with shorter B–Ti and C–Ti bonds. To investigate the interactions between the impurity and matrix atoms, we calculated the Mulliken populations of the impurity and adjacent matrix atoms, as shown in Table 2. In pure TiO_2, the Mulliken populations of the O and Ti atoms are −0.66 and 1.33, respectively. But in the doped TiO_2, the Mulliken populations of all Ti atoms bonded to the B and C atoms are smaller than 1.33, attributed to the weaker electronegativities of the B and C atoms than those of the O atoms. Therefore, the reduced charge

Table 2 Mulliken populations on the impurity and adjacent matrix atoms in the supercells of the B-, C- and B/C-doped anatase TiO_2[a]

				O population		Ti population	
No.	Doped TiO_2	B population	C population	Bonded to B	Bonded to C	Bonded to B	Bonded to C
(a)	B_O	−0.29				1.19(2)[b]	
(b)	B_{Ti}	0.77		−0.61			
				−0.64			
				−0.67			
				−0.68			
(c)	B_i	0.67		−0.69(4)			
(d)	C_O		−0.45				1.23(2)
							1.28
(e)	C_{Ti}		0.83		−0.44(2)		
(f)	C_i		−0.11				
(g)	B_OC_O	−0.08	−0.61			1.19(2)	1.23(3)
(h)	$B_{Ti}C_{Ti}$	0.80	0.68	−0.69	−0.56(2)		
				−0.70(2)	−0.58		
(i)	B_iC_i	0.69	−0.13	−0.70(4)	−0.52		1.20
					−0.58		1.27
							1.32
(j)	B_OC_{Ti}	−0.11	0.66	−0.63	−0.53	1.20	
					−0.60		
					−0.61		
(k)	$B_{Ti}C_O$	0.77	−0.25	−0.60	−0.52		
				−0.64			1.20
				−0.68			1.32
				−0.69			
(l)	B_OC_i	−0.57	0.60		−0.55	1.06(2)	
					−0.57(2)	1.08	
(m)	B_iC_O	0.69	−0.68	−0.69			1.18(2)
				−0.70(3)			1.19
(n)	$B_{Ti}C_i$	0.76	0.23	−0.60	−0.58		1.22
				−0.66	−0.59		
				−0.68	−0.60		
				−0.69			
(o)	B_iC_{Ti}	0.70	0.38	−0.69(2)	−0.48		
				−0.70(2)			

[a] In the pure anatase TiO_2: O population = −0.66, Ti population = 1.33. [b] The numbers in the parentheses describe the quantity of atoms with same Mulliken population.

transfer between impurity atoms and Ti atoms causes weaker and longer bonds (B–Ti and C–Ti).

It should be noted that the change regulation of Mulliken populations of O atoms is different from that of Mulliken populations of Ti atoms in the B-, C- and B/C-doped anatase TiO_2. Table 2 indicates that the Mulliken populations of O atoms are about −0.66. Further observation indicates that the Mulliken populations of the O atoms bonded to C atoms are lower than −0.66, while O atoms bonded to B atoms show higher Mulliken populations than O atoms bonded to C atoms, which originates from the larger electronegativity of the C atom than the B atom. In addition, the B_O atom always plays a role of an anion with negative Mulliken population, while the B_{Ti} and B_i atoms act as cations with positive Mulliken population. The C_O and C_{Ti} atoms are similar to the B_O and B_{Ti} atoms, respectively. But the C_i atoms show negative Mulliken population in the C_i–TiO_2 and B_iC_i–TiO_2 and positive Mulliken population in the B_OC_i–TiO_2 and $B_{Ti}C_i$–TiO_2. Consequently, both doping atoms and their doping positions influence the lattice structure of doped TiO_2 together.

3.2 Formation energies

To compare the relative stabilities of all doped anatase TiO_2 models, the formation energy was calculated. The formation energies of doped TiO_2 were calculated by the following formula:[25]

$$E_{form} = E_{doped} - E_{pure} - m\mu_B - n\mu_C + x\mu_O + y\mu_{Ti} \quad (1)$$

where E_{doped} is the total energy of the doped TiO_2 supercell and E_{pure} is the total energy of the pure TiO_2 supercell. μ_B and μ_C are the chemical potentials of B and C atoms, respectively. μ_O (μ_{Ti}) is the chemical potential of the O (Ti) atom. The coefficients m and n are the numbers of B and C atoms doped into the supercells of TiO_2, respectively. The x and y represent the numbers of O and Ti atoms substituted by impurity atoms, respectively. It should be mentioned that the formation energy is not fixed but depends on the growth condition, which can be changed from O-rich to Ti-rich (O-poor). The relations between μ_O and the chemical potentials of other atoms (B, C and Ti) are as follows:

$$3\mu_O + 2\mu_B = \mu(B_2O_3) \quad (2)$$

$$2\mu_O + \mu_C = \mu(CO_2) \quad (3)$$

$$2\mu_O + \mu_{Ti} = \mu(TiO_2) \quad (4)$$

where the space group of B_2O_3 is $P31$. Under O-rich growth conditions, the O chemical potential μ_O is calculated from the

Table 3 Formation energies (eV) for the B-, C- and B/C-doped anatase TiO_2

No.	Doped TiO_2	O-rich	Ti-rich	No.	Doped TiO_2	O-rich	Ti-rich
(a)	B_O	17.06	4.13	(i)	B_iC_i	17.80	−0.30
(b)	B_{Ti}	2.33	4.91	(j)	B_OC_{Ti}	15.74	2.81
(c)	B_i	8.10	0.34	(k)	$B_{Ti}C_O$	13.20	0.27
(d)	C_O	14.40	−1.11	(l)	B_OC_i	24.94	1.68
(e)	C_{Ti}	4.40	4.40	(m)	B_iC_O	18.80	−4.47
(f)	C_i	12.88	2.54	(n)	$B_{Ti}C_i$	9.27	1.51
(g)	B_OC_O	29.32	0.89	(o)	B_iC_{Ti}	10.79	3.04
(h)	$B_{Ti}C_{Ti}$	3.70	6.28				

Table 4 The E_v, E_c, E_g and E_{max} for the pure, B-, C- and B/C-doped anatase TiO_2

No.	Doped TiO_2	E_v (eV)	E_c (eV)	E_g (eV)	E_{max} (eV)	No.	Doped TiO_2	E_v (eV)	E_c (eV)	E_g (eV)	E_{max} (eV)
	Pure	6.20	8.32	2.12	2.12	(h)	$B_{Ti}C_{Ti}$	2.89	5.49	2.60	2.60
(a)	B_O	4.53	6.70	2.17	1.55	(i)	B_iC_i	3.80	6.63	2.83	1.26
(b)	B_{Ti}	3.49	5.79	2.30	2.30	(j)	B_OC_{Ti}	2.63	5.39	2.76	1.74
(c)	B_i	4.61	7.08	2.47	2.47	(k)	$B_{Ti}C_O$	3.46	5.91	2.45	1.37
(d)	C_O	4.91	7.12	2.21	0.76	(l)	B_OC_i	3.44	6.08	2.64	1.96
(e)	C_{Ti}	4.94	6.88	1.94	1.94	(m)	B_iC_O	3.81	6.31	2.50	1.20
(f)	C_i	3.82	6.41	2.59	1.51	(n)	$B_{Ti}C_i$	3.63	6.07	2.44	1.49
(g)	B_OC_O	3.55	6.14	2.59	0.84	(o)	B_iC_{Ti}	3.30	5.78	2.48	1.89

ground-state energy of the O_2 molecule ($\mu_O = \mu(O_2)/2$), while the B, C and Ti chemical potentials are determined by the formulae (2), (3) and (4), respectively. Under Ti-rich growth conditions, the Ti chemical potential μ_{Ti} is obtained from the energy of one Ti atom in bulk Ti ($\mu_{Ti} = \mu_{bulk\text{-}Ti}$) and the O chemical potential μ_O is determined by the formula (4). Then μ_B and μ_C are also calculated by the formulae (2) and (3), respectively. Consequently, the formation energy can be looked as the function of O chemical potential μ_O. Table 3 exhibits the formation energies of all doped supercells under the O-rich and Ti-rich growth conditions. It can be clearly seen that O-rich conditions favor the formation of B_{Ti}–TiO_2, C_{Ti}–TiO_2 and $B_{Ti}C_{Ti}$–TiO_2, while Ti-rich conditions easily promote the growth of other doped TiO_2. This confirms that the impurity atoms prefer to replace the Ti atom under O-rich growth conditions, contrarily, they tend to substitute the O atom and occupy the interstitial position under Ti-rich growth conditions. Especially, the B_iC_O–TiO_2 is the most stable doped system due to its lowest formation energy (−4.47 eV) under Ti-rich growth conditions. This is also consistent with some reported experimental results,[17a,18] indicating the existence of B–O and C–Ti bonds (see Fig. 2m). Further observation shows that the formation energies of co-doped TiO_2 are lower than the total formation energies of corresponding single-doped TiO_2, indicating that the B/C-doping method can further reduce the formation energy of the impurity atom in the co-doped TiO_2. Considering the relationship between E_{form} and μ_O, different B-, C- and B/C-doped anatase TiO_2 can be easily prepared by controlling O_2 pressure. This is also proved to be efficient in other doped models.[25,26] To further investigate the photocatalytic activities of doped TiO_2 growing under different O_2 conditions, we discuss the electronic properties of all the B-, C- and B/C-doped anatase TiO_2 in the next section.

3.3 Electronic properties

To analyze the modifications of electronic properties and clarify the origin of enhanced visible-light photocatalytic activity in degradation of organic pollutants, the band structures and projected density of states (PDOS) of pure and doped anatase TiO_2 were calculated. The calculated band structures and PDOS are plotted in Fig. 3. Based on the plots of calculated band structures, the E_v, E_c, E_g and E_{max} (the maximum energy gap in the band gap) of pure and doped TiO_2 are also listed in Table 4.

For the pure anatase TiO_2, the conduction band mostly consists of Ti 3d states and the valence band is composed of Ti 3d and O 2p states. The calculated band gap of the pure anatase TiO_2 is 2.12 eV, lower than the experimental value of 3.20 eV. This is due to the known limitation of DFT. Table 4 indicates that the band gaps of all the doped TiO_2 except the C_{Ti}–TiO_2 are wider than that of pure TiO_2. This makes the absorption edges of the doped TiO_2 shift to the ultraviolet region. However, the impurity states in the band gaps significantly decrease the maximum energy gap (E_{max}), thus resulting in the visible light absorption of doped TiO_2. For single-doped TiO_2, the 2p states of the B_O and C_O atoms are both localized in the band gaps (see Fig. 3a and d). However, no impurity state appears in the band gaps of the B_{Ti}–TiO_2 and C_{Ti}–TiO_2 (see Fig. 3b and e). This is well consistent with some DFT studies.[19] But the B_i and C_i atoms have completely different performance in the band gaps. The one 2s state and one 2p state of the C_i atom are localized above the top of the valence band and below the bottom of the conduction band (see Fig. 3f), respectively. But the 2s and 2p states of the B_i atom are not found in the band gap. Surprisingly, the distributing regulations of the 2p states of B_O, B_{Ti}, B_i and C_O atoms in the single-doped TiO_2 also apply to the B/C-doped TiO_2. But the distances from impurity states to the edges of band gaps are changed. As for C_{Ti} and C_i, the 2s and 2p states of C_i disappear in the band gap of the B_OC_i–TiO_2, while the 2s and 2p states of the C_{Ti} atom appear in the band gap of the B_iC_{Ti}–TiO_2. It can be seen that the doping of B atoms leads to redistributions of the 2s and 2p states of C_{Ti} and C_i atoms. Hence, the impurity states located in the band gap are not only related to the location of the impurity atom, but also depend on the chemical environment around the impurity atom.

As a typical semiconductor, the Fermi level of pure TiO_2 is just above the top of the valence band and its conduction band is empty without any electron. But in some band structure plots of doped TiO_2, the Fermi levels move into the conduction bands, resulting in the metallic properties. As a result, some Ti 3d states at the bottom of conduction bands are occupied by the electrons, indicating that the Ti^{4+} ions are reduced to the Ti^{3+} ions. The above analysis on the Mulliken populations of Ti atoms bonded to impurity atoms also exhibits similar results. That is, the Mulliken populations of Ti atoms in doped TiO_2 is lower than 1.33 of pure TiO_2, implying the increase of electron density and enhancement in reducibility of Ti atoms in doped TiO_2. Fig. 3 indicates that the Ti 3d states at the bottom of conduction bands have

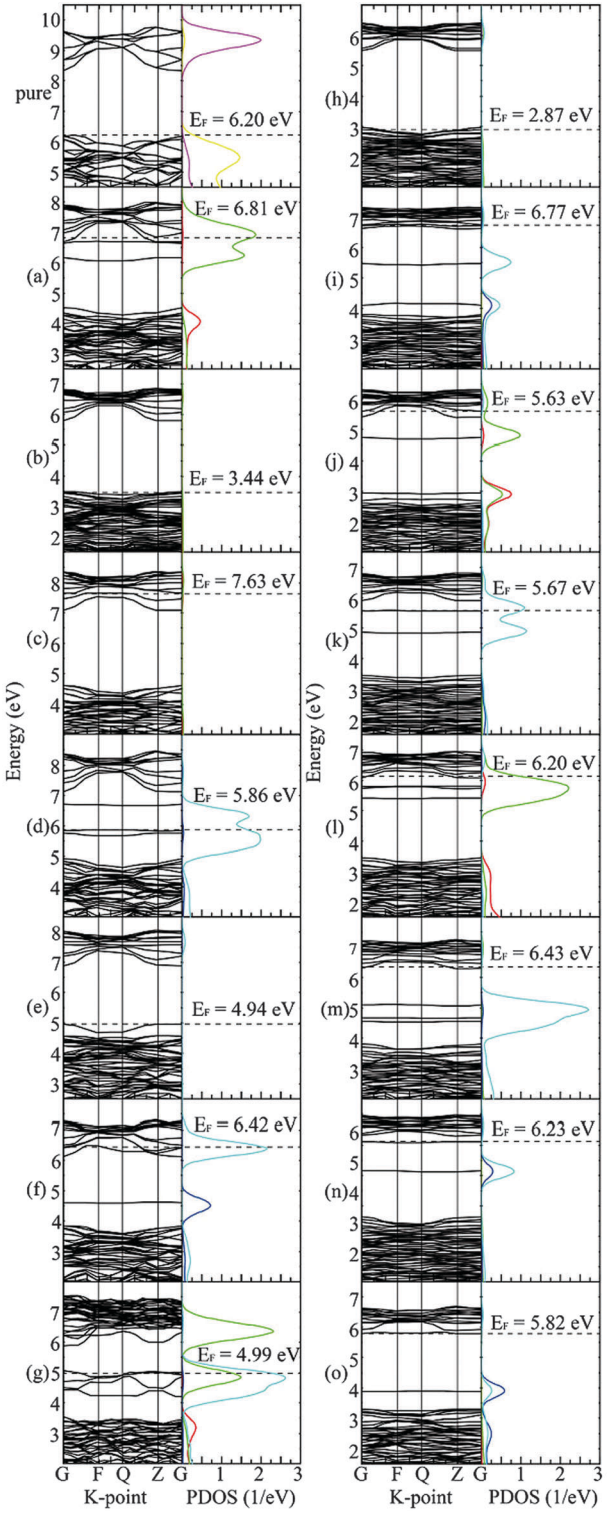

Fig. 3 Band structures and projected density of state (PDOS) plots for all simulated systems. To compare the E_v and E_c of different simulated systems, all energies from the CASTEP are raised by the corresponding E_F. The dashed lines in the band structures represent the Fermi level (E_F). The yellow lines stand for the PDOS of O 2p, magenta for Ti 3d, red for B 2s, green for B 2p, blue for C 2s and cyan for C 2p.

greater curvatures than the O 2p states at the top of valence bands, implying that the conduction electrons have lower efficient masses and higher velocities according to the following formulae:

$$m^* = \pm (h/2\pi)^2 (\mathrm{d}^2E/\mathrm{d}k^2)^{-2} \quad (5)$$

$$v = hk/2\pi m^* \quad (6)$$

where m^* is the efficient mass, h is the Planck constant, k is the wave vector, E is the energy of wave vector k and v is the velocity. Therefore, it is not surprising that the electrons in the Ti^{3+} 3d states easily transfer to the acceptor (O_2). Meanwhile, the photogenerated electron easily jumps to the conduction band from the valence band or the impurity state and continues to occupy the empty Ti^{3+} 3d state under light irradiation. However, the photogenerated holes left in the valence bands or the impurity states accept the electron from the donor (such as OH^- and H_2O). Therefore, the 3d state of the Ti^{3+} ion is the highly efficient separation center of photogenerated electrons and holes. To our knowledge, many previous studies also indicate that the Ti^{3+} ions can reduce the recombination of photogenerated electrons and holes and enhance photocatalytic activity.[19d,27] In addition, like the distributions of impurity states, the locations of Fermi levels also depend on the doping modes. In the B_{Ti}–TiO_2, C_{Ti}–TiO_2 and $B_{Ti}C_{Ti}$–TiO_2 (see Fig. 3b, e and h), the Fermi levels still stay at the top of valence bands. However, the Fermi levels move into the band gaps in the C_O–TiO_2, B_OC_O–TiO_2 and $B_{Ti}C_O$–TiO_2 (see Fig. 3d, g and k). For other doped TiO_2, Fermi levels enter the bottom of conduction bands. It is evident that the interstitial atom can push the Fermi level into the bottom of conduction bands, mainly due to the extra electrons from the impurity atoms easily transferring to the Ti atoms.

Further observation from Fig. 3 and Table 4 indicates that the valence and conduction bands of all doped TiO_2 move down to the low energy region compared with those of pure TiO_2. The decreased values of E_v and E_c are more than 1.20 eV (see Table 4). Moreover, B and C co-doping of TiO_2 results in larger decreased values of E_v and E_c compared with single-doped TiO_2. It is well known that the photogenerated holes in the lower energy states have a better oxidizability and the photogenerated electrons in the higher energy states have a stronger reducibility. Therefore, the oxidizability of photogenerated holes at the top of valence bands is enhanced and the reducibility of photogenerated electrons at the bottom of conduction bands is reduced in the doped TiO_2. During the photocatalytic degradation of an organic pollutant, the O_2 on the surface of TiO_2 is oxidized by the photogenerated electron to the O_2^- ion, while the OH^- on the surface of TiO_2 is reduced by the photogenerated hole to the $^\bullet$OH radical. The O_2^- ion, the hole and the $^\bullet$OH radical all are important oxidants in the photocatalytic degradation. As a result, the doped TiO_2 tends to generate more $^\bullet$OH radicals than O_2^- ions. Our recent investigation results also indicated that the hole and the derived $^\bullet$OH radical played a dominant role in the visible-light photocatalytic degradation of RhB for the B/C-doped TiO_2.[18] This also further supports the above theoretical calculations and discussions.

4. Conclusions

The visible-light absorption and photocatalytic activities of the B-, C- and B/C-doped anatase TiO_2 are studied using the DFT calculations of the first-principles. The stabilities of the doped TiO_2 depend on its growth conditions (O-rich or Ti-rich environment). The O-rich growth condition is beneficial to the formation of B_{Ti}–TiO_2, C_{Ti}–TiO_2 and $B_{Ti}C_{Ti}$–TiO_2, while the Ti-rich growth condition is favorable to the preparation of other doped TiO_2 including the most stable B_iC_O–TiO_2. The energy gaps (E_g), the distributions of impurity states, the locations of Fermi levels (E_F) and the energies of the edges of band gaps have a synergetic influence on the visible-light absorption and photocatalytic activity of the doped TiO_2. The impurity states located at the band gaps reduce the maximum energy gaps of the band gaps and enhance the absorption of visible light. The Ti^{3+} ions induced by Fermi levels located at the bottom of conduction bands promote the separation of photogenerated electrons and holes. The valence bands and conduction bands of the B-, C- and B/C-doped anatase TiO_2 move toward the low energy region, resulting in the stronger oxidizability of photogenerated holes at the top of valence bands and weaker reducibility of photogenerated electrons at the bottom of conduction bands. Furthermore, the B/C-doped TiO_2 possesses the partial electronic properties of single-doped TiO_2, but also presents many new electronic properties, indicating that the electronic properties of co-doped TiO_2 are not simply a mechanical mixture of those of both B and C single-doped TiO_2. This investigation will provide some new insights into design and synthesis of the multi-doped TiO_2 with the predicted electronic properties by controlling the growth conditions.

Acknowledgements

This work was partially supported by the 973 program (2013CB632402), 863 Program (2012AA062701), NSFC (51072154, 21177100 and 51272199) and Natural Science Foundation of Hubei Province (2010CDA078). Also, this work was financially supported by the Fundamental Research Funds for the Central Universities and Self-Determined and Innovative Research Funds of SKLWUT.

Notes and references

1 A. Fujishima and K. Honda, *Nature*, 1972, **238**, 37.

2 (*a*) Y. Xu and M. A. A. Schoonen, *Am. Mineral.*, 2000, **85**, 543; (*b*) E. Borgarello, R. Pappa, N. Serpone and E. Pelizzetti, *Photocatal. Environ.*, 1988, 567; (*c*) D. Brinkley and T. Engel, *J. Phys. Chem.*, 1998, **102**, 7596; (*d*) M. R. Hoffmann, S. T. Martin, W. Choi and D. W. Bahnemann, *Chem. Rev.*, 1995, **95**, 69; (*e*) Q. J. Xiang, J. G. Yu and M. Jaroniec, *Chem. Soc. Rev.*, 2012, **41**, 782; (*f*) G. P. Dai, J. G. Yu and G. Liu, *J. Phys. Chem. C*, 2012, **116**, 15519; (*g*) K. L. Kv, B. Cheng, J. G. Yu and G. Liu, *Phys. Chem. Chem. Phys.*, 2012, **14**, 5349.

3 (*a*) M. Anpo, H. Yamashita, Y. Ishihashi, Y. Fujii and M. Honda, *J. Phys. Chem.*, 1997, **101**, 2632; (*b*) T. Inoue, A. Fujishima, S. Konishi and K. Honda, *Nature*, 1979, **277**, 637; (*c*) M. Kanemoto, H. Hosokawa, Y. Wada, K. Murakoshi, S. Yanagida, H. Mori, M. Ishikawa and H. Kobayashi, *J. Chem. Soc.*, 1996, **92**, 2401.

4 (*a*) I. Lauermann, D. Meissner and R. Memming, *J. Electroanal. Chem.*, 1987, **228**, 45; (*b*) J. Reber and K. Meier, *J. Phys. Chem.*, 1984, **88**, 5903; (*c*) J. Zhang, J. G. Yu, Y. M. Zhang, Q. Li and J. R. Gong, *Nano Lett.*, 2011, **11**, 4774; (*d*) Q. J. Xiang, J. G. Yu and M. Jaroniec, *J. Am. Chem. Soc.*, 2012, **134**, 6575; (*e*) J. Zhang, J. G. Yu, M. Jaroniec and J. R. Gong, *Nano Lett.*, 2012, **12**, 4584.

5 (*a*) V. Augugliaro, L. Palmisano, C. Minero and E. Pelliezzetti, *Environ. Toxicol. Chem.*, 1988, **16**, 89; (*b*) R. I. Bickley, J. A. Navio, R. K. M. Jayanty and V. Vishwanathan, *Photocatal. Environ.*, 1988, 683; (*c*) G. N. Schrauzer and T. D. Guth, *J. Am. Chem. Soc.*, 1977, **99**, 7189; (*d*) J. Soria, J. C. Conesa, V. Augugliaro, L. Palmisano, M. Schiavello and A. Sciafani, *J. Phys. Chem.*, 1991, **95**, 274.

6 (*a*) S. W. Liu, J. G. Yu and M. Jaroniec, *J. Am. Chem. Soc.*, 2010, **132**, 11914; (*b*) J. G. Yu, S. W. Liu and H. G. Yu, *J. Catal.*, 2007, **249**, 59; (*c*) J. G. Yu, Y. R. Su and B. Cheng, *Adv. Funct. Mater.*, 2007, **17**, 1984; (*d*) Q. J. Xiang, J. G. Yu and M. Jaroniec, *Chem. Commun.*, 2011, **47**, 4532.

7 (*a*) J. G. Yu, G. P. Dai and B. B. Huang, *J. Phys. Chem. C*, 2009, **113**, 16394; (*b*) Q. J. Xiang, J. G. Yu, W. G. Wang and M. Jaroniec, *Chem. Commun.*, 2011, **47**, 6906.

8 (*a*) X. X. Yang, C. D. Cao, L. Erickson, K. Hohn, R. Maghirang and K. Klabunde, *Appl. Catal., B*, 2009, **91**, 657; (*b*) R. Asahi, T. Morikawa, T. Ohwaki, K. Aoki and Y. Taga, *Science*, 2001, **293**, 269; (*c*) F. F. Li, Y. S. Jiang, M. S. Xia, M. M. Sun, B. Xue, D. R. Liu and X. G. Zhang, *J. Phys. Chem. C*, 2009, **113**, 18134; (*d*) X. H. Tang and D. Y. Li, *J. Phys. Chem. C*, 2008, **112**, 5405; (*e*) Q. J. Xiang, J. G. Yu and M. Jaroniec, *Phys. Chem. Chem. Phys.*, 2011, **13**, 4853; (*f*) L. Kumaresan, M. Mahalakshmi, M. Palanichamy and V. Murugesan, *Ind. Eng. Chem. Res.*, 2010, **49**, 1480; (*g*) A. Mattsson, M. Leideborg, L. Persson, G. Westin and L. Österlund, *J. Phys. Chem. C*, 2009, **113**, 3810; (*h*) H. Irie, Y. Wanatabe and K. Hashimoto, *J. Phys. Chem. B*, 2003, **107**, 5483; (*i*) J. C. Yu, J. G. Yu, W. K. Ho, Z. T. Jiang and L. Z. Zhang, *Chem. Mater.*, 2002, **14**, 3808; (*j*) S. W. Liu, J. G. Yu and W. G. Wang, *Phys. Chem. Chem. Phys.*, 2010, **12**, 12308.

9 (*a*) R. Plass, S. Pelet, J. Krueger, M. Gratzel and U. Bach, *J. Phys. Chem. B*, 2002, **106**, 7578; (*b*) S. G. Hickey, D. J. Riley and E. J. Tull, *J. Phys. Chem. B*, 2000, **104**, 7623; (*c*) I. Robel, M. Kuno and P. V. Kamat, *J. Am. Chem. Soc.*, 2007, **129**, 4136; (*d*) I. Robel, V. Subramanian, M. Kuno and P. V. Kamat, *J. Am. Chem. Soc.*, 2006, **128**, 2385; (*e*) W. T. Sun, Y. Yu, H. Y. Pan, X. F. Gao, Q. Chen and L. M. Peng, *J. Am. Chem. Soc.*, 2008, **130**, 1124; (*f*) L. F. Qi, J. G. Yu and M. Jaroniec, *Phys. Chem. Chem. Phys.*, 2011, **13**, 8915.

10 S. U. M. Khan, M. Al-shahry and W. B. Ingler Jr., *Science*, 2002, **297**, 2243.

11 S. Sakthivel and H. Kisch, *Angew. Chem., Int. Ed.*, 2003, **42**, 4908.

12 H. Kamisaka, T. Adachi and K. Yamashita, *J. Chem. Phys.*, 2005, **123**, 084704.
13 (*a*) Y. Park, W. Kim, H. Park, T. Tachikawa, T. Majima and W. Choi, *Appl. Catal., B*, 2009, **91**, 355; (*b*) X. X. Yang, C. D. Cao, K. Hohn, L. Erickson, R. Maghirang, D. Hamal and K. Klabunde, *J. Catal.*, 2007, **252**, 296; (*c*) B. Zhou, M. Schulz, H. Y. Lin, S. I. Shah, J. H. Qu and C. P. Huang, *Appl. Catal., B*, 2009, **92**, 41; (*d*) I. C. Kang, Q. W. Zhang, S. Yin, T. Sato and F. Saito, *Appl. Catal., B*, 2008, **80**, 81.
14 (*a*) M. Bettinelli, V. Dallacasa, D. Falcomer, P. Fornasiero, V. Gombac, T. Montini, L. Romanò and A. Speghini, *J. Hazard. Mater.*, 2007, **146**, 529; (*b*) A. Zaleska, E. Grabowska, J. W. Sobczak, M. Gazda and J. Hupka, *Appl. Catal., B*, 2009, **89**, 469; (*c*) A. Zaleska, J. W. Sobczak, E. Grabowska and J. Hupka, *Appl. Catal., B*, 2008, **78**, 92; (*d*) R. Khan, S. W. Kim, T. J. Kim and C. M. Nam, *Mater. Chem. Phys.*, 2008, **112**, 167.
15 (*a*) J. G. Yu, G. P. Dai, Q. J. Xiang and M. Jaroniec, *J. Mater. Chem.*, 2011, **21**, 1049; (*b*) S. W. Liu, C. Li, J. G. Yu and Q. J. Xiang, *CrystEngComm*, 2011, **13**, 2533.
16 S. Sakthivel and H. Kisch, *ChemPhysChem*, 2003, **4**, 487.
17 (*a*) Y. M. Wu, M. Y. Xing, J. L. Zhang and F. Chen, *Appl. Catal., B*, 2010, **97**, 182; (*b*) Y. M. Wu, M. Y. Xing and J. L. Zhang, *J. Hazard. Mater.*, 2011, **192**, 368.
18 J. G. Yu, Q. Li, S. W. Liu and M. Jaroniec, *Chem.–Eur. J.*, 2013, **19**, 2433.
19 (*a*) K. S. Yang, Y. Dai and B. B. Huang, *J. Phys. Chem. C*, 2010, **114**, 19830; (*b*) K. S. Yang, Y. Dai, B. B. Huang and M. H. Whanbo, *J. Phys. Chem. C*, 2009, **113**, 2624; (*c*) H. T. Gao, C. H. Ding and D. M. Dai, *THEOCHEM*, 2010, **944**, 156; (*d*) C. D. Valentin, G. Pacchioni and A. Selloni, *Chem. Mater.*, 2005, **17**, 6656.
20 N. Serpone, *J. Phys. Chem. B*, 2006, **110**, 24287.
21 M. D. Segall, P. L. D. Lindan, M. J. Probert, C. J. Pickard, P. J. Hasnip, S. J. Clark and M. C. Payne, *J. Phys.: Condens. Matter*, 2002, **14**, 2717.
22 J. P. Perdew, K. Burk and M. Ernzerhof, *Phys. Rev. Lett.*, 1996, **77**, 3865.
23 J. P. Perdew and Y. Wang, *Phys. Rev. B: Condens. Matter Mater. Phys.*, 1992, **45**, 13244.
24 H. J. Monkhorst and J. D. Pack, *Phys. Rev. B: Condens. Matter Mater. Phys.*, 1976, **13**, 5188.
25 R. Long and N. J. English, *J. Phys. Chem. C*, 2009, **113**, 8373.
26 K. S. Yang, Y. Dai and B. B. Huang, *J. Phys. Chem. C*, 2007, **111**, 12086.
27 C. D. Valentin, E. Finazzi and G. Pacchioni, *Chem. Mater.*, 2008, **20**, 3706.